Int. J. Heat Mass Transfer. Vol. 34, No. 9, pp. 2175–2186, 1991
Printed in Great Britain

0017–9310/91 $3.00 + 0.00

Influence of an array of wall-mounted cylinders on the mass transfer from a flat surface

M. K. CHYU
Department of Mechanical Engineering, Carnegie Mellon University, Pittsburgh, PA 15213, U.S.A.

and

R. J. GOLDSTEIN
Department of Mechanical Engineering, University of Minnesota, Minneapolis, MN 55455, U.S.A.

(*Received* 6 *June* 1990 *and in final form* 16 *October* 1990)

Abstract—An experimental study is performed to investigate the effects of two arrays—in-line and staggered—of cylinders on the mass transfer from a flat surface on which the cylinders are situated. Both arrays have seven rows of short (height-to-diameter ratio of unity) cylinders and identical transverse and longitudinal pitches. The naphthalene sublimation technique, in association with an automated, computer controlled naphthalene surface measurement system gives detailed local mass transfer information. The distributions of local mass transfer coefficient reveal the details of establishment of a periodic regime as well as recurring local maxima and minima. Characteristics of mass transfer from the region immediately adjacent to the base of a cylinder in an array are comparable to that around a single, isolated cylinder. Area-averaged mass transfer results, obtained from numerical integration (summation) of the local data, provide a direct, region-by-region comparison between the two arrays. The arrays produce mass transfer enhancement from the surface of approximately 46 and 53% for the in-line and the staggered arrays, respectively.

INTRODUCTION

HEAT TRANSFER from arrays of cylinders in cross flow has been extensively investigated in the past because of its importance in a wide range of heat exchanger applications. Early work focused on the configuration of circular tube banks with relatively large values of tube length-to-diameter ratio [1]. The primary heat transfer area lies on the cylindrical surfaces, and the heat transfer on the endwalls and the endwall effects on the tube surface heat transfer are of secondary importance. Other important configurations relating to cylinder arrays are compact heat exchangers of fin-and-tube type [2] and the short pin fins located near the trailing edge inside a turbine blade [3,4]. In these cases, the main flow normal to cylinder arrays is constrained between closely spaced endwalls (typically one diameter apart) attached to the cylinders. As contrasted to the transport to a long tube bank, with short cylinders a large fraction of the total heat transfer will occur on the endwalls rather than primarily on the tubes themselves. It is expected that the distribution of heat transfer on an endwall surface is strongly dependent on the geometry of the cylinder array.

Characteristics of heat transfer from a wall-mounted array of cylinders are closely related to the flow pattern in the region near the base of cylinders where strong cylinder–endwall interaction occurs. As fluid flows over a wall-mounted cylinder, the boundary layer in the near wall region separates three-dimensionally and creates a number of vortex-pairs rolling over and/or sweeping around the cylinder base. The name, horseshoe vortex, often referring to this flow field (particularly for a long cylinder), is based on the envelope shape of the main vortex. Previous studies have demonstrated that the horseshoe vortex in fact consists of many vortices with complex interactions and oscillatory motions [5].

A horseshoe vortex produces high wall shear stress beneath it which, in turn, yields high heat or mass transfer from the wall. Earlier work includes studies by Kruckels [6] and Jones and Russell [7] who studied the local mass transfer distributions on annular fins. Goldstein *et al.* recently studied the local mass transfer characteristics from the cylinder surface [8] as well as the endwall [9]. In these studies, the naphthalene sublimation technique was implemented with a high-precision, computer-automated, measurement system to obtain detailed local mass transfer rate. Very non-uniform local mass transfer distributions are observed on both the cylinder and endwall with several local maxima and minima. It has been reported that the ratio of cylinder height-to-diameter, H/D, significantly affects the mass transfer in the wake region behind a cylinder. However, the mass transfer in front of a cylinder is rather insensitive to the cylinder height.

The flow field associated with a wall-mounted array of cylinders is more complex than that with a single

NOMENCLATURE

D cylinder diameter, 6.35 mm in present study
H height of rib or cylinder, 6.35 mm in present study
h_m naphthalene mass transfer coefficient, equation (2)
L total length of mass transfer active surface in the X-direction, 377.4 mm
$\dot{m}$ mass transfer flux of naphthalene from surface
$p_{v,w}$ naphthalene vapor pressure at wall
Re Reynolds number based on cylinder diameter, $U_\infty D/\nu = 1.68 \times 10^4$ in present study
S_L longitudinal distance for cylinder array, Fig. 1
S_T transverse distance for cylinder array, Fig. 1
Sc naphthalene-to-air mass transfer Schmidt number
St mass transfer Stanton number from naphthalene surface, h_m/U_∞
St_l average Stanton number over the length of mass transfer surface in the X-direction; a function of Z for surface with cylinders situated on it, $(1/L)\int_0^L St\, dX$
St_0 mass or heat transfer Stanton number from flat surface, a function of X
St_{0l} average St_0 over the length L for the flat surface, $(1/L)\int_0^L St_0\, dX$
St_{0R} average of St_0 for a given row of the flat surface, $(1/S_L)\int_{X_{CL}-S_L/2}^{X_{CL}+S_L/2} St_0\, dX$
St_R average Stanton number on wall surface for a given row of cylinders for surfaces with cylinders situated on it, $(1/(2S_T \cdot S_L))\int_{X_{CL}-S_L/2}^{X_{CL}+S_L/2}\int_{S_T/2}^{S_T} St\, dZ\, dX$
St_T average Stanton number across span in the Z-direction; a function of X for surfaces with cylinders situated on it, $(1/S_T)\int_{S_T/2}^{S_T} St\, dZ$
t time
U_∞ velocity of freestream, 38.4 ± 0.3 m s^{-1} in present study
X streamwise coordinate, Fig. 1
X_{CL} X location of center line for a row of cylinders
y distance measured from reference plane down to position on naphthalene surface, equation (4)
Z lateral distance across span measured from the symmetry line of measurement domain.

Greek symbols
ρ_s density of solid naphthalene, 1.143 g cm^{-3}
$\rho_{v,w}$ naphthalene vapor mass concentration at wall
ρ_∞ naphthalene vapor mass concentration in freestream, zero in present study.

cylinder. The additional important parameters are related to array configuration. In-line and staggered arrays are the most common, and they can be geometrically specified by the relative longitudinal and transverse pitches, S_L/D and S_T/D (Fig. 1). The flow and heat transfer around a cylinder in the first row of an array are generally expected to be similar to that around isolated cylinders, but would vary with array configurations in the downstream rows. In the present study, two seven-row arrays of cylinders are used, an in-line array and a staggered array. For a rational comparison, identical geometrical parameters; i.e. H/D, S_L/D and S_T/D, are used for both arrays. Figure 1 displays schematic views of the array geometries and coordinate system.

Conventional thermal experimental methods are in general unable to provide data with a high degree of accuracy and fine grid for studies of local heat transfer on a surface over which there is a large variation in heat transfer coefficient. A mass transfer system using the naphthalene ($C_{10}H_8$) sublimation technique is used for the present study. The shaded regions shown in Fig. 1, coated with naphthalene, represent the mass transfer active surfaces on the flat endwalls. The cylinders are made of brass and are mass transfer inactive. Local mass transfer coefficients on the naphthalene surfaces are measured in great detail using an automated, microcomputer-controlled measurement system. Features of this measurement system have been reported earlier [9]. The mass transfer results may be transformed into their heat transfer counterparts using a principle of analogy between the two transfer processes [10]. The following briefly describes the data reduction of the present mass transfer system.

DATA REDUCTION

The mass transfer coefficient, h_m, is given by

$$h_m = \dot{m}/(\rho_{v,w} - \rho_\infty) \quad (1)$$

where $\dot{m}$ is the mass transfer rate per unit area, and $\rho_{v,w}$ and ρ_∞ the naphthalene vapor concentrations near the wall and in the freestream, respectively. The present study approximates a boundary layer situation with $\rho_\infty = 0$. Equation (1) thus becomes

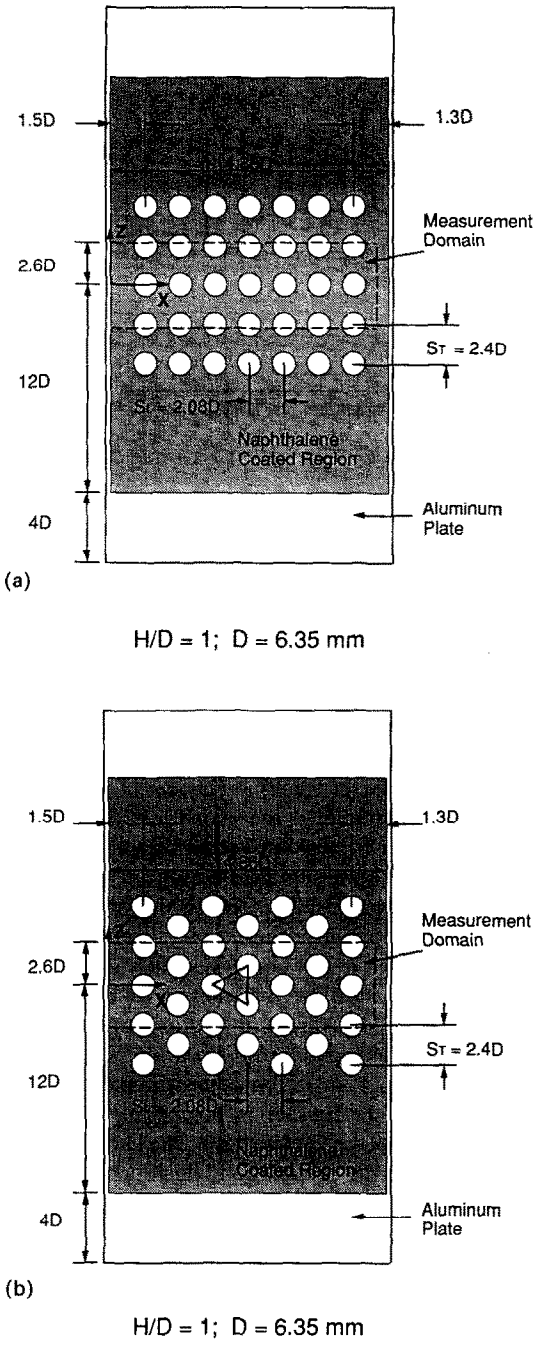

FIG. 1. Test plate and coordinate system: (a) in-line; (b) staggered.

$$h_m = \dot{m}/\rho_{v,w}. \quad (2)$$

Local mass transfer from a naphthalene surface is determined from the change in naphthalene thickness

$$dy/dt = \dot{m}/\rho_s \quad (3)$$

where ρ_s is the density of solid naphthalene. Note that dy and $\dot{m}$ depend on the position on the subliming surface. Combining equations (2) and (3), and integrating over the test duration yields the time-averaged local mass transfer coefficient

$$h_m = (\rho_s \cdot \Delta y)/(\rho_{v,w} \cdot \Delta t). \quad (4)$$

The dimensionless mass transfer coefficient, the Stanton number, is

$$St = h_m/U_\infty. \quad (5)$$

As the wall temperature often varies slightly during a test run, $\rho_{v,w}$ is represented by the time-averaged naphthalene concentration at the surface. This is calculated from the numerically integrated concentration determined at the measured surface temperature. A correlation [11] is used to determine the naphthalene vapor pressure; from this, $\rho_{v,w}$ is evaluated using the ideal gas law and the naphthalene surface temperature.

EXPERIMENTAL APPARATUS AND PROCEDURE

Experiments were carried out in a specially designed open-circuit wind tunnel (5.24 m in total length) operated in a suction mode. The tunnel consists of an entrance section which includes screens and flow straighteners followed by a contraction section, a test section, a diffuser section, a blower and a discharge duct. During the experiment, room air is induced through the tunnel and blown out of the laboratory into the adjacent service corridor. The building ventilation system then exhausts the discharge into the atmosphere, ensuring the tunnel inlet air to be free from naphthalene vapor. A general sketch of the tunnel is shown in Fig. 2. A detailed description of the tunnel can be found in ref. [12]. At the end of the contraction section, a 2 mm diameter steel rod is placed on the bottom wall of the section, across the tunnel span and normal to the mean flow direction, to serve as a boundary layer trip. For all of the test runs, the freestream velocity is maintained nearly constant at 38.4 m s^{-1} in the test section. The Reynolds number based on this freestream velocity and the diameter (D) of the cylinders is about 1.6×10^4.

The test section has a rectangular cross section, 203 mm wide and 152 mm high. It is made of acrylic plastic (Plexiglas) with a thickness of 19 mm for the side walls and 12.7 mm for the top and the bottom. To provide additional mechanical strength and to maintain its straightness, the Plexiglas walls are further braced by a 19 mm thick aluminum frame. A portion of the bottom wall is removed and replaced by a naphthalene test plate during the mass transfer experiments.

The test plate, shown in Fig. 1, is made of 19 mm thick aluminum tooling plate. The central portion on one of the surfaces is machine-cut with a nominal 3.2 mm recession to provide space for casting of the naphthalene layer. The casting is made by implanting molten, nearly boiling, naphthalene into the recession with the designated mass transfer surface faced against highly polished aluminum plate. Holes are

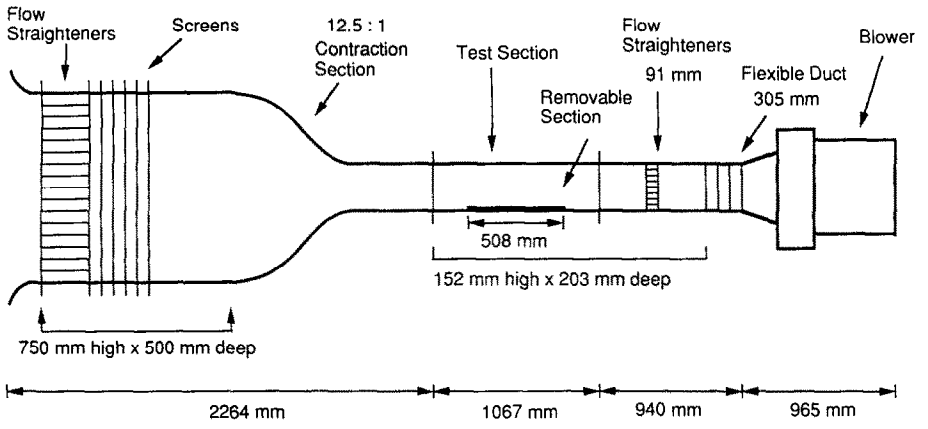

FIG. 2. Test section and wind tunnel.

drilled through the test plate at positions where cylinders are to be located. All cylinders are made of brass rod and have identical dimensions, 6.4 mm in diameter and height. To facilitate a cylinder standing on the naphthalene coated plate, an inward-tapered teflon annulus is inserted into the base hole of each cylinder prior to the naphthalene casting. The outer diameter of the teflon annulus is equal to that of a cylinder, and the inner wall, tapped with screw threads, has a 3.2 mm diameter. During the casting of naphthalene, the inserted annulus blocks the flow of molten naphthalene and adheres to the surrounding solidified naphthalene afterwards. One end of each cylinder is machined to screw into the inner wall of the annulus, ensuring a firm support.

As previously mentioned and also shown in Fig. 1, both arrays use an identical longitudinal and transverse pitch, $S_T/D = 2.40$ and $S_L/D = 2.08 = (\sqrt{3}/2)S_T/D$. One of the arrays can be obtained by shifting the even number rows of the other array sideways by one-half transverse pitch. Equilateral triangles are formed between axes of any three neighboring but not aligned cylinders for the staggered array. Although both arrays have seven rows of cylinders, the total number of cylinders mounted on the test plate is different. For the in-line array, each row consists of five cylinders with 35 cylinders in total. For the staggered array, the number of cylinders per row is alternated with five in the odd number rows and four in the even number rows giving a total of 32 cylinders.

The naphthalene surface begins $1.5D$ (9.5 mm) upstream from the axes of the first row of cylinders and ends at $1.3D$ (8.3 mm) downstream from the last row's axes. A local planar coordinate system X–Z is specified as illustrated in Fig. 1. Note X represents the downstream distance, Z the lateral distance across the span, and Y the normal distance from the X–Z plane. The entire naphthalene coated area can be described as $0.0 \leqslant X/D \leqslant 14.86$ and $-12.0 \leqslant Z/D \leqslant 12.0$. The area bounded by dotted lines, $0.0 \leqslant X/D \leqslant 14.8$ and $-2.6 \leqslant Z/D \leqslant 2.6$, represents the region where the local mass transfer measurement is performed. Note that the transverse span of the measurement domain is slightly larger than twice the transverse pitch of cylinder arrays ($Z/D \leqslant |2.6|$ vs $S_T/D = 2.4$). Furthermore, approximately 15% of the area in the measurement domain is underneath the cylinders, and thus is mass transfer inactive. The size of this 'active surface' area reduction is the same for both arrays.

To calculate the local mass transfer coefficient, the depth of naphthalene sublimed during a test period at a certain location must be determined. The difference in the local naphthalene surface elevations measured before and after a test run gives such a depth. If detailed local transport information is required, a large number of measurement locations must be used so that a sufficient spatial resolution can be achieved. This implies that an effective measurement system should have high accuracy in positioning capability and rapid rate in data acquisition. The latter is essential to alleviate the sublimation which occurs during the measurement procedures outside the test time. To fulfill all these requirements, the system described in ref. [9] is used. This is an automated, computer-controlled, naphthalene surface measurement system which consists of a depth gauge, a two-axis stepper-motor driven positioner, a stepper-motor controller, and a microcomputer. The depth gauge has a precision of 2.5×10^{-5} mm (1 micro-inch) and the positioner is capable of addressing the X–Z plane with a minimum of 2.5×10^{-2} mm (1 mil) increment in each direction. The measurement time between two consecutive data points, which is the accumulative duration for the positioner movements, the stabilization of the depth probe and the data transmission and storage, is approximately 2 s.

Within the measurement domain indicated in Fig. 1, any two adjacent data points, for both arrays, are uniformly spaced with a 1.27 mm ($0.2D$) increment along both the X- and Z-directions. This results in 75 and 27 points along the X- and Z-axis, respectively,

and a total of 2025 data points. In addition, another set of local mass transfer data is also acquired at the middle of the longitudinal pitch between rows and with a much larger span, i.e. $-5.2 \leqslant Z/D \leqslant 5.2$. This provides more detailed mass transfer variation in the spanwise and the row-resolved directions.

RESULTS AND DISCUSSION

Most of the mass transfer results are presented in terms of St/St_0—a normalized index representing the influence of a cylinder or the array on the mass transfer from a flat wall. St_0 is obtained using measurements made on a flat naphthalene plate without the cylinders in the same tunnel operating with the same flow conditions. St_0 shows power law dependency on the streamwise coordinate (X/D) of the type $St_0 = 1.62 \times 10^{-3}(X/D)^{-0.19}$. The equation compares favorably with correlations for heat transfer from a flat wall to a turbulent boundary layer with zero free-stream pressure gradient, though the absolute values of St_0 are somewhat smaller. This is attributed to the inactive-mass-transfer starting length. This agreement provides confidence in the present experimental system. The uncertainty in the local Stanton number based on the analysis in ref. [12] is about 4%.

Figures 3 and 4 show contour plots of St/St_0 for the in-line and the staggered array, respectively. Each figure contains two parts, (a) and (b), for easier data presentation and comparison. Parts (a) and (b) plot St/St_0 contours with a 0.5 increment and start from $St/St_0 = 1.0$ to 3.0 and 1.25 to 2.75, respectively. The contours in (a) and (b) of the corresponding figure can all be plotted on a single figure if a finer contour increment or more contour lines are desired. Very non-uniform and distinct distributions of St/St_0 are observed from these sets of contour plots. Mass transfer in the region immediately ahead and alongside of every cylinder is rather insensitive to the array geometry, and has very similar characteristics to the mass transfer near a single cylinder [9]. In these regions, values of St/St_0 are high and local maxima exist.

Downstream of a cylinder, the mass transfer is strongly influenced by the array pattern. One primary difference between the two arrays is that a local maximum and a minimum of St/St_0 exist along the symmetry line behind each cylinder for the staggered array; while, for the in-line array, St/St_0 along the symmetric line (through the cylinders) increases almost linearly from the rear surface of a cylinder to the region immediately ahead of a cylinder in the subsequent row. The downstream maximum St/St_0 for the staggered array occurs approximately at $1.0D$ from the cylinder's rear surface, and the minimum occurs at about $1.0D$ further downstream from the

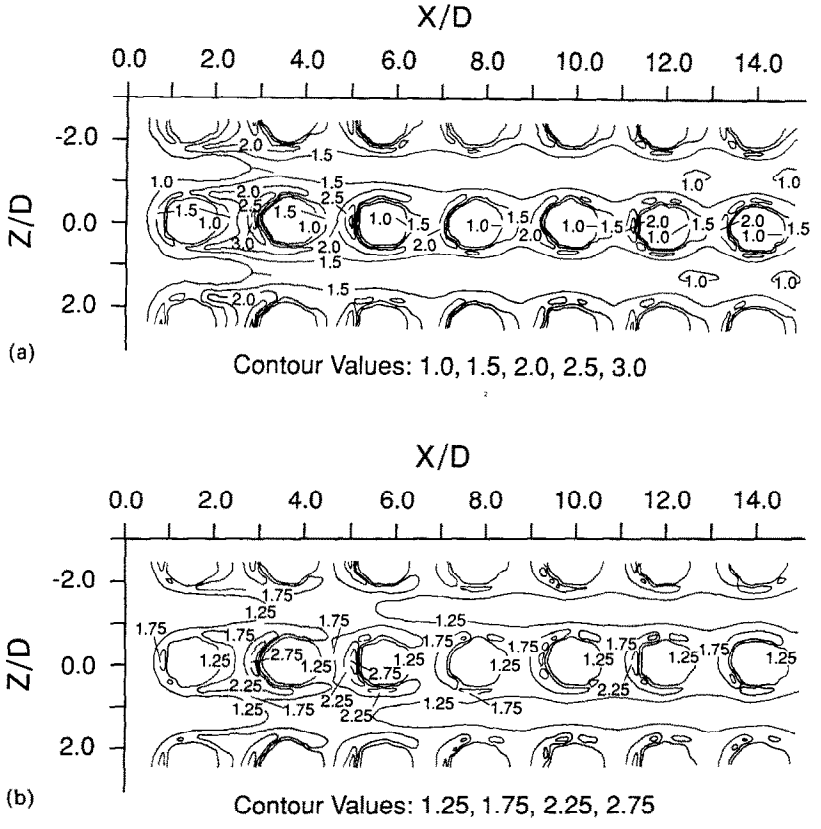

FIG. 3. Local mass transfer distribution for in-line array: (a) $St/St_0 = 1.0, 1.5, 2.0, 2.5, 3.0$; (b) $St/St_0 = 1.25, 1.75, 2.25, 2.75$.

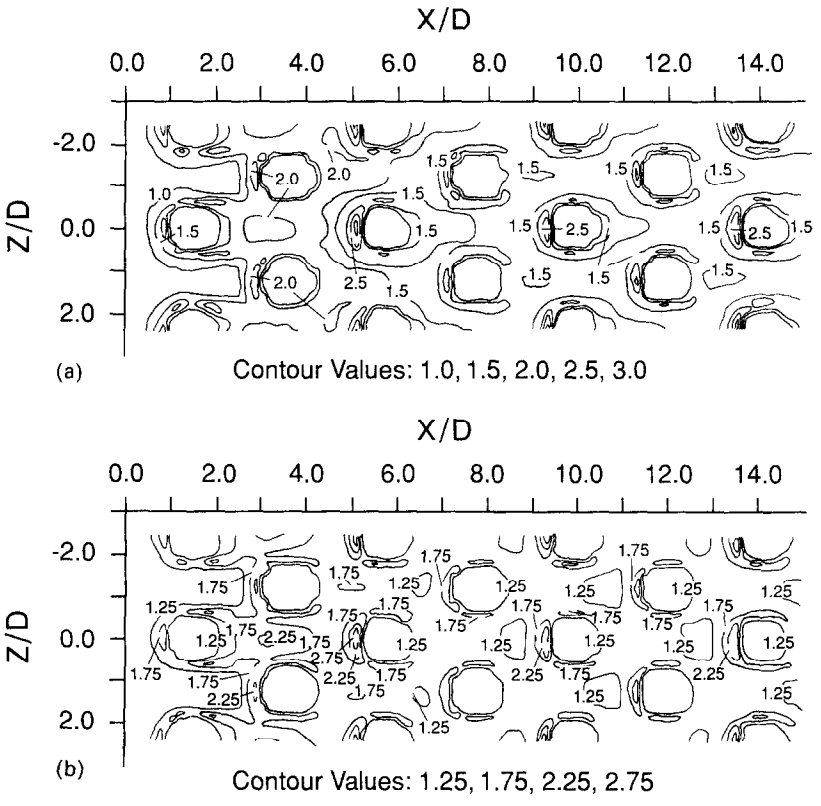

FIG. 4. Local mass transfer distribution for staggered array: (a) St/St_0 = 1.0, 1.5, 2.0, 2.5, 3.0; (b) St/St_0 = 1.25, 1.75, 2.25, 2.75.

maximum. The magnitudes of these maxima and minima St/St_0 vary with the cylinder row number. The highest maximum St/St_0 occurs behind the first row, with a value of approximately 2.25 (Fig. 4(b)). The value of maximum St/St_0 then decreases progressively for the second and third row, and it finally remains as a constant at 1.5 after the third row (Fig. 4(a)). The minimum St/St_0 also has the highest value at 1.5 behind the first row. It then decreases with the row number and reaches a constant of 1.25 after the third row (Fig. 4(b)). This mass transfer variation between rows will also be shown later in Figs. 5 and 6.

The difference in the flow field caused by the array geometry accounts for the aforementioned difference of the mass transfer variation between the two arrays. A study [9] on single cylinders has suggested that the characteristics of mass transfer downstream of a cylinder are strongly influenced by whether the separated shear layer over a cylinder top reattaches to the flat surface downstream. For an array of cylinders, the existence of such a reattachment is primarily a function of S_L/D (or longitudinal pitch), H/D, and flow conditions. A comparison between Figs. 3 and 4 suggests that the value of $S_L/D = 2.08$ appears to be too short to permit the flow reattachment behind a cylinder for the in-line array. Nevertheless, the staggered array has effectively doubled the longitudinal pitch so that the mass transfer behind a cylinder reveals the effects of reattachment.

Further examination of Figs. 3 and 4 shows mass transfer coefficients near the first row of cylinders for both arrays are comparable and similar to that of a single cylinder [9]. A significant change of mass transfer starts from the second row. Notwithstanding the different detailed distributions of St/St_0, both arrays experience distinctly high mass transfer near the second row. For the staggered array, the separated shear layer from the first row reattaches in the space between two transversely adjacent cylinders of the second row. This produces a high mass transfer in this region. In addition, a cylinder in the second row is at the exit of a channel formed between two transversely adjacent cylinders in the first row. The impingement of such an accelerating flow is also believed to be responsible for the high mass transfer in front of second-row cylinders. However, for the in-line array, these effects are not present. With the longitudinal pitch ($S_L/D = 2.08$) used in the present study, the longitudinal gap between adjacent cylinders would have been filled completely with recirculating vortices shedding from the cylinder upstream. Flow through the unobstructed section is thus comparable with flow in a straight channel. The region near the second row can be feasibly regarded as an entrance section for the channel. A high mass transfer coefficient near a channel entrance is expected.

Downstream of the first two rows, the aforementioned entrance effect is alleviated, and the mech-

anism of mass transfer is considered to be comprised of two counteracting effects. As an approaching boundary layer flows over the top of a cylinder row, the cylinders generate stronger turbulence in the near-wall region and also thicken the boundary layer. Compared with flow over a smooth wall, the turbulence increases the mass transfer from the wall, while the thicker boundary layer produces greater transfer resistance. The presence of the cylinders introduces additional surface resistance to the flow, and fluid in the near-wall region tends to migrate toward the core-flow or the freestream. This results in a thick boundary layer.

Also observed in Figs. 3 and 4 is that, for both arrays, mass transfer from the fourth row and further downstream reveals a near-periodic pattern between rows. This is characterized by the repeat of local maxima and minima of St/St_0. The implication is that the net effect of combined increases in turbulence and boundary layer thickness, as previously mentioned, on St as a function of X/D is similar to the decreasing trend of St_0 vs X/D. For the in-line array, as shown in Fig. 3(a), several locations in the unobstructed region near the sixth row and downstream have values of St/St_0 slightly less than unity. This is possible due to uncertainties involved in the experiment or the correlation of St_0 used. Another speculation is that the flow acceleration near the unobstructed region causes the boundary layer to re-laminarize, and this, in turn, results in a lower mass transfer coefficient.

Figures 5 and 6 present the transverse distributions of St/St_0 at every mid-pitch of adjacent rows. Similar measurements are also taken at $S_L/2$ upstream of the first row and downstream of the last row. The results are symmetric with respect to $Z = 0$. Mass transfer at $S_L/2$ before the first row for both arrays shows the behavior of a flat wall boundary layer; $St/St_0 \sim 1.0$ at this location. For all the data downstream of the first row, the mid-pitch St/St_0 always achieves a local maximum right behind a cylinder and a local minimum at the middle of a transverse pitch. This trend is observed for both arrays. Starting downstream of the third row, the mid-pitch St/St_0 shows a periodic profile which repeats every row for the in-line and every other row for the staggered, respectively. It is conceivable to assert that the mass transfer in both array configurations achieves the periodic condition near the third row, although, as expected, the staggered array seems to have slightly longer developing length than the in-line array. Overall this is in good agreement with results of several heat or mass transfer studies on short-cylinder arrays in confined channels [3,13,14].

The highest local maximum of St/St_0 at mid-pitch occurs downstream of the first row; it is about 30% higher than the maxima of downstream rows. This highest maximum is somewhat greater with the in-line array than with the staggered array. In addition, an irregular and more divergent maximum is present for the in-line array, in contrast to a clear peak for the staggered array.

The mass transfer characteristics near the (transverse) sides of an array are different from those in the central region. The effect appears to be stronger for the staggered array than for the in-line array, as evidenced by a significant increase of St/St_0 at both sides of the third, fifth and seventh rows for the staggered array. The flow around these cylinders is less constrained by neighboring cylinders and a stronger separation–reattachment effect results in relatively high mass transfer.

Simoneau and VanFossen [15] presented turbulence data along the mid-line of longitudinal pitch for flow over an in-line and a staggered array of cylinders. The study was performed in a confined channel flow with $S_L/D = S_T/D = 2.67$, and $H/D = 0.5$ and 2.0. Despite the different geometries and operating conditions, the profiles of the present mid-pitch St/St_0 are similar to those of turbulence intensity in ref. [15]. Turbulence intensity is also found to be high near the

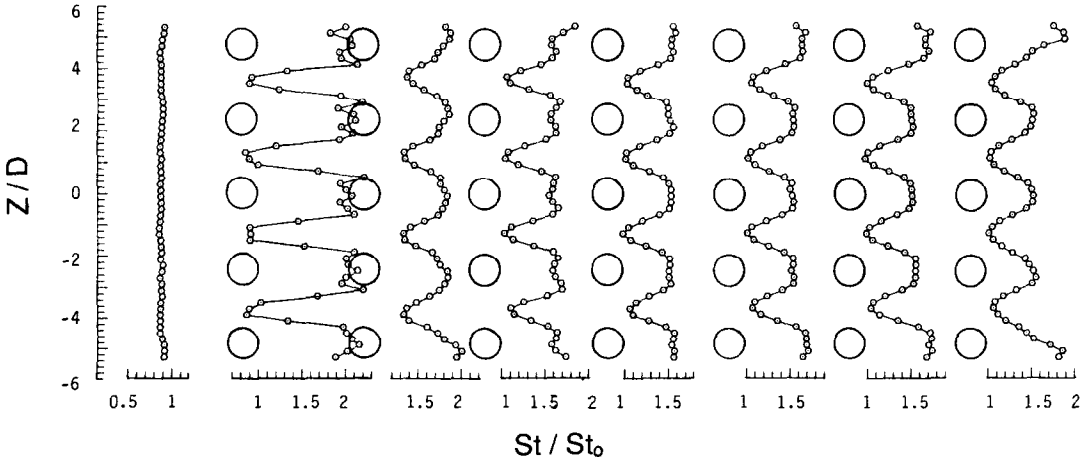

FIG. 5. Longitudinal mass transfer variation at mid-pitch for in-line array.

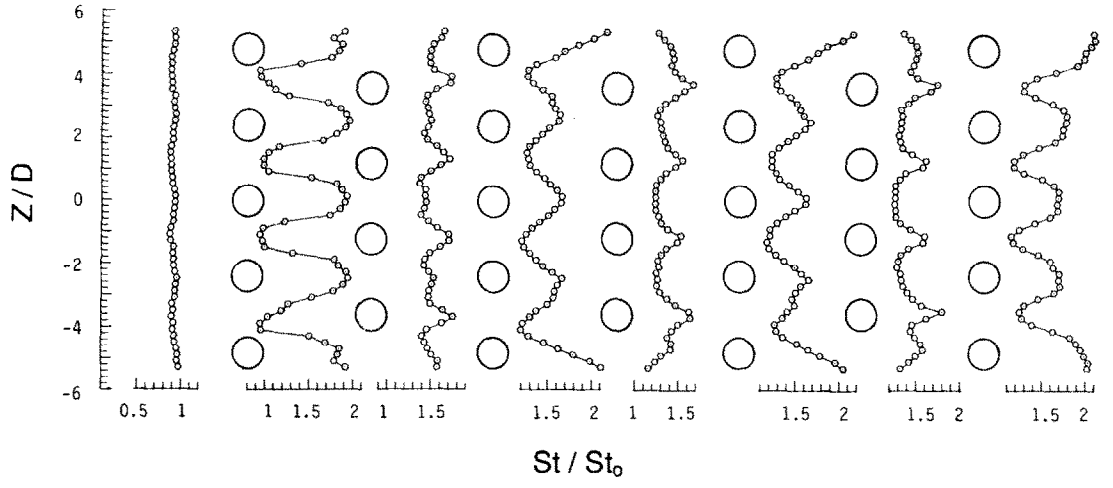

FIG. 6. Longitudinal mass transfer variation at mid-pitch for staggered array.

transverse end of a staggered array. A high turbulence level is expected to result in high mass transfer.

The area-averaged mass transfer results are calculated using Simpson's rule for both one- and two-dimensional integrations. The area covered by cylinder bases is about 15% of the total domain of interest, so the area-averaged results depend on whether the mass transfer inactive area covered by cylinder bases is counted in the averaging or not. Results for both area-averages are presented for comparison. Figure 7 shows the spanwise (transverse) averaged mass transfer coefficient in the form of St_T/St_0 based on the area ($-1.2 \leqslant Z/D \leqslant 1.2$ and $0 \leqslant X/D \leqslant 14.86$) in which the cylinder covered area (having $St = 0$) is counted in the averaging. Figure 8 is the counterpart of Fig. 7, with only the mass transfer active area being averaged. Figures 9 and 10 provide a comparison between the two different averaged results for each individual array. Using averaging procedures corresponding to those of Figs. 7 and 8, respectively, Figs. 11 and 12 show the distribution of streamwise (longitudinal) averaged, spanwise-resolved mass transfer coefficient, St_L/St_{0L} ($0 \leqslant X/D \leqslant 14.86$, $-2.4 \leqslant Z/D \leqslant 2.4$). Figure 13 presents the row-by-row averaged mass transfer, St_R/St_{0R} ($-S_L/2 \leqslant X_{CL}/D \leqslant S_L/2$, $-2.4 \leqslant Z/D \leqslant 2.4$) vs row number. The area underneath a cylinder is counted in the averaging calculation for Fig. 13.

As shown in Figs. 7 and 8, the spanwise mass transfer St_T/St_0 is comparable between the two arrays. A local maximum of St_T/St_0 exists immediately ahead of a cylinder. This is well expected as the local data of Figs. 3 and 4 are high in the region ahead of a cylinder. Clear periodic (with X/D) variation St_T/St_0 distribution begins at the third row, the first two rows having a stronger variation of St_T/St_0 with X/D. Variation of St_T/St_0 near the last row appears to be different from the periodic behavior that prevails in the upstream rows. This is believed to be caused by the absence of cylinders downstream, which, in turn, results in a strong separation–reattachment effect.

The general trend of St_T/St_0, shown in Figs. 7 and 8, can be described as follows. Starting from the maximum ahead of a cylinder row, St_T decreases with X/D, reaching a minimum near the middle of the row, and then increases downstream until the maximum just ahead of the next row is reached. The increasing trend, in fact, includes a plateau of St_T/St_0 that occurs

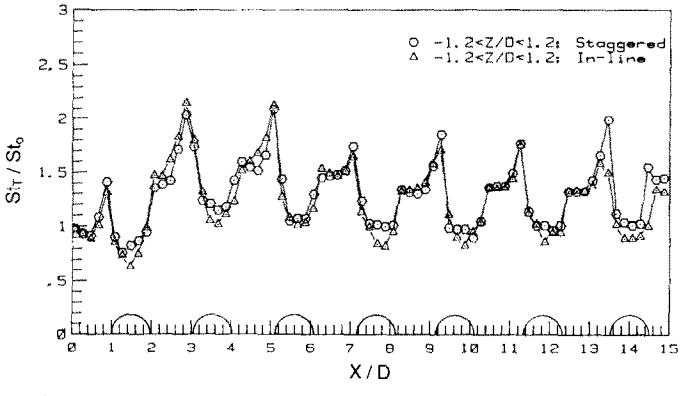

FIG. 7. Spanwise average mass transfer distribution; averaged with cylinder-base covered area.

in the void region between two adjacent rows. The plateau effect is quite clear after the third row where the periodic characteristic starts to prevail. However, it becomes rather insignificant if only the mass transfer active area is averaged, as shown in Fig. 8. The results in Figs. 9 and 10 reveal that St_T/St_0 based on two different averaging areas differ by 30–50% in regions where the cylinders are located.

As seen in Figs. 11 and 12, local maxima of streamwise mass transfer, St_L/St_{0L}, exist in regions very close to the cylinders. The horseshoe vortices, wrapping around the cylinder and then extending further downstream, are responsible for those mass transfer maxima. Excluding the cylinder's side maxima, St_L/St_{0L} for the staggered array remains somewhat constant across the span. On the other hand, for the in-line array, Fig. 11 shows local minima at the symmetric line of cylinder axes ($Z/D = 0$) and at the middle of the transverse pitch. The latter obviously is because of the aforementioned channel effect in the cylinder-unobstructed regions. The former is attributed to the large size of mass transfer inactive area

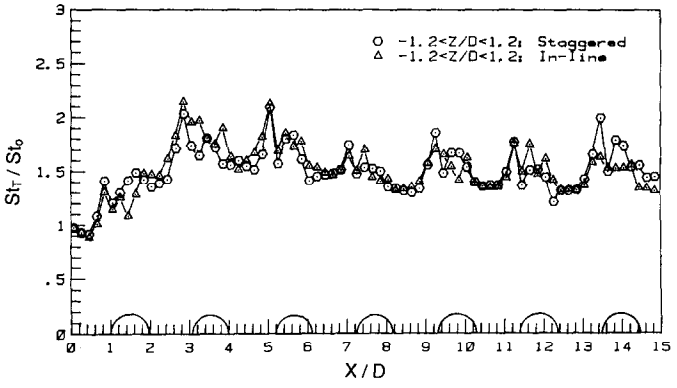

FIG. 8. Spanwise average mass transfer distribution; averaged without cylinder-base covered area.

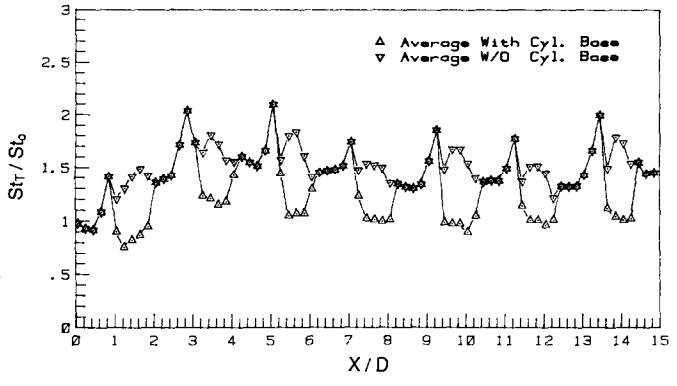

FIG. 9. Spanwise average mass transfer distribution; in-line array.

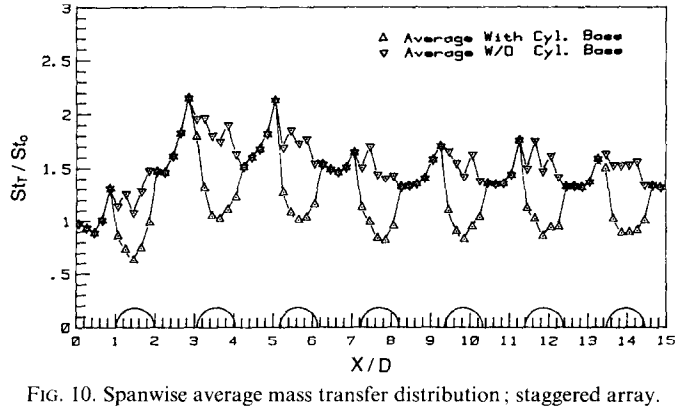

FIG. 10. Spanwise average mass transfer distribution; staggered array.

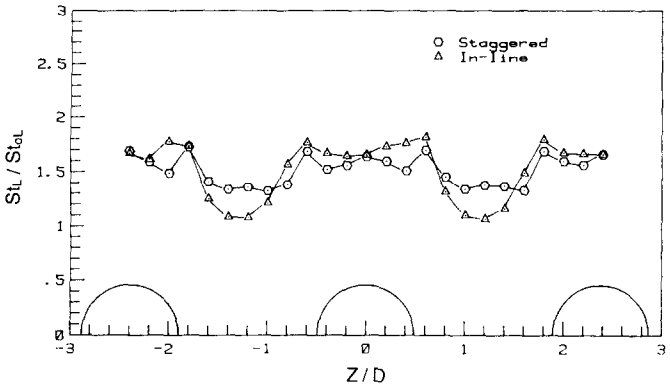

FIG. 11. Streamwise average mass transfer distribution; averaged with cylinder-base covered area.

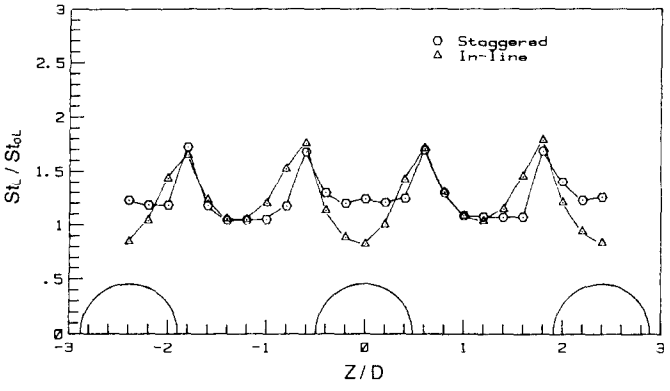

FIG. 12. Streamwise average mass transfer distribution; averaged without cylinder-base covered area.

counted in the averaging calculation. The results present in Fig. 12, excluding the mass transfer inactive area, clarify this viewpoint as values of St_L/St_{0L} near $Z/D = 0$ are approximately twice as high as the corresponding values shown in Fig. 11.

Row-by-row averaged mass transfer, St_R/St_{0R}, is shown in Fig. 13. This row-resolved mass transfer is based on the area confined within a half longitudinal pitch upstream and downstream from a cylinder axis. As mentioned earlier, the mass transfer inactive area underneath a cylinder is counted in the averaging. The general trend in St_R/St_{0R} for both arrays is an initial

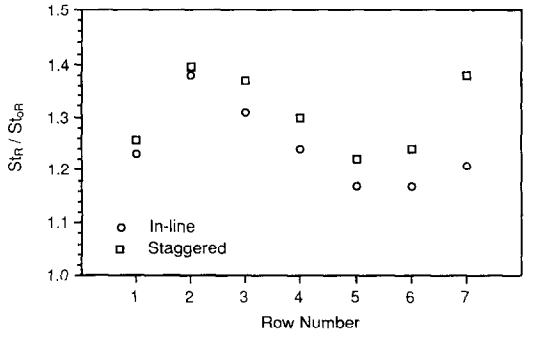

FIG. 13. Row-by-row average mass transfer; averaged with cylinder-base covered area.

increase in the first two rows, reaching a clear maximum at the second row and followed by a subsequent decline between the third and the fifth rows. St_R/St_{0R} then rises again in the last two rows. This is believed to be largely caused by the end effects of the array and will be described later. St_R/St_{0R} for the first two rows is affected little by the difference in array configuration, but in the subsequent rows, it is always larger for the staggered array than for the in-line array. The difference is about 5% for the third to fifth rows and is about 20% for the last row. Distinction in array geometry towards the last row segregates the associated flow pattern and transfer behavior unlike that which prevails in the inner rows. The last two rows of cylinders in the staggered array appear to experience a stronger separation–reattachment effect so that higher mass transfer is produced. To a certain extent, only the last row of the in-line array is subjected to such a difference, because no reattachment behind a cylinder will take place for the inner rows of the in-line array, as previously concluded. The exit effect is therefore weaker compared to the staggered array.

The most comparable row-resolved averaged studies found in the literature were carried out by Metzger *et al.* [3] and, more recently, by Chyu [14]. Results reported in these two studies are qualitatively in agree-

ment with the present findings. Depending on the Reynolds number, the maximum row-by-row mass (heat) transfer occurs at about the second to fifth row followed by a gradual decline in heat transfer through the remainder of the array.

Averaged mass transfer over the entire test surface for both in-line and staggered arrays can be calculated from data shown in Fig. 13. The overall average increase in mass transfer is 1.24 for the in-line array and 1.30 for the staggered array. These values are obtained with the inclusion of the total area covered by cylinder bases. Excluding this area, the results will be 1.46 and 1.53, respectively. It therefore appears that, under the present operating conditions, the staggered array is a better device than the in-line array if enhancement of mass or heat transfer is the main concern. However, according to ref. [14], with similar array geometries, a staggered array in general produces a higher friction loss than an in-line array. Therefore, if a higher enhancement index, defined as the enhancement of mass transfer per penalty of friction loss, the in-line array may be more favorable.

CONCLUSIONS

The effect of wall-mounted arrays of short cylinders on the local mass transfer from a flat surface have been studied in detail. The distributions of local mass transfer coefficient reveal the details of transition from a developing to a periodic regime. For both arrays studied, a very high mass transfer occurs within the first two rows of cylinders, while the periodic condition is reached near the third row. The mass transfer coefficient in close vicinity to the base of each cylinder in both arrays is high, and it appears uninfluenced by the array geometry. However, mass transfer in the relatively unobstructed region around the cylinders depends greatly on the array geometry. The in-line array experiences low mass transfer in the unobstructed region between two transversely adjacent cylinders, particularly in the downstream rows. On the other hand, local maxima and minima of mass transfer are present in the staggered array. Area-averaged mass transfer results, obtained from integration of local data, provide a direct, region-by-region comparison between the two arrays. Both arrays produce mass transfer enhancement from the surface, approximately 46 and 53% for the in-line and staggered array, respectively. The difference in enhancement between the two arrays occurs primarily in the periodic regime; the magnitudes of the average mass transfer results in the entrance regions in these two arrays are similar.

REFERENCES

1. A. Zukauskas, Heat transfer from tubes in crossflow. In *Advances in Heat Transfer*, Vol. 8. Academic Press, New York (1972).
2. F. E. M. Saboya and E. M. Sparrow, Local and average transfer coefficients for one-row plate fin and tube heat exchanger configurations, *J. Heat Transfer* **97**, 265–272 (1974).
3. D. E. Metzger, R. A. Berry and J. P. Bronson, Developing heat transfer in rectangular ducts with staggered arrays of short pin fins, *J. Heat Transfer* **104**, 700–706 (1982).
4. J. Armstrong and D. Winstanley, A review of staggered array pin fin heat transfer for turbine cooling applications, ASME Paper 87-GT-201 (1987).
5. L. S. Langston and M. T. Boyle, A new surface-streamline flow-visualization technique, *J. Fluid Mech.* **125**, 53–58 (1982).
6. W. W. Kruckels, Determination of local heat transfer coefficients in forced air flow by aid of photometric measurements, *A.I.Ch.E. Symp. Ser.* **68**, 112–118 (1972).
7. T. V. Jones and M. B. Russell, Heat transfer in annular fins, ASME Paper 78-HT-30 (1978).
8. R. J. Goldstein and J. Karni, The effects of a wall boundary on local mass transfer for a cylinder in cross-flow, *J. Heat Transfer* **106**, 260–267 (1984).
9. R. J. Goldstein, M. K. Chyu and R. C. Hain, Measurement of local mass transfer on a surface in the region of the base of a protruding cylinder with a computer-controlled data acquisition system, *Int. J. Heat Mass Transfer* **28**, 977–985 (1985).
10. E. R. G. Eckert, Analogies to heat transfer processes. In *Measurements in Heat Transfer* (Edited by E. R. G. Eckert and R. J. Goldstein). Hemisphere, New York (1976).
11. D. Ambrose, I. J. Lawenson and C. H. S. Sprake, The vapor pressure of naphthalene, *J. Chem. Thermo.* **7**, 1173–1176 (1975).
12. M. K. Chyu, Influence of roughness elements on the mass transfer from a flat surface, Ph.D. Thesis, University of Minnesota (1986).
13. E. M. Sparrow, J. W. Ramsey and C. A. C. Altemani, Experiments on in-line pin fin arrays and performance comparisons with staggered arrays, *J. Heat Transfer* **102**, 44–50 (1980).
14. M. K. Chyu, Heat transfer and pressure drop for short pin-fin arrays with pin-endwall fillet, *J. Heat Transfer* **112**, 926–932 (1990).
15. R. J. Simoneau and G. J. VanFossen Jr., Effect of location in an array on heat transfer to a short cylinder in crossflow, *J. Heat Transfer* **106**, 42–48 (1984).

INFLUENCE SUR LE TRANSFERT DE MASSE D'UNE RANGEE DE CYLINDRES MONTES EN PAROI PLANE

Résumé—Une étude expérimentale est montée pour connaître les effets de deux rangées de cylindres, en ligne ou en quinconce, sur le transfert de masse à partir d'une surface plane sur laquelle sont montés ces cylindres. Les rangées ont sept cylindres courts (hauteur = diamètre) et des pas transverses et longitudinaux identiques. La technique de sublimation du naphtalène, en associant un système automatique de contrôle de la surface de naphtalène, donne une information détaillée du transfert local de masse. Les distributions du coefficient local de transfert donnent les détails de l'établissement d'un régime périodique et d'une recurrence de maximums et minimums locaux. Les caractéristiques du transfert de masse à partir de la région immédiatement adjacente à la base du cylindre dans une rangée sont comparables à celles autour d'un cylindre isolé unique. Des résultats de transfert de masse moyennés sur la surface, obtenus par intégration numérique (sommation) des données locales, fournissent une comparaison directe région par région entre les deux rangées. Celles-ci produisent un accroissement du transfert de masse sur la surface respectivement d'environ 46 et 53% pour les arrangements en ligne et en quinconce.

EINFLUSS EINER ANORDNUNG AUS ZYLINDRISCHEN RIPPEN AUF DEN STOFFÜBERGANG AN EINER EBENEN OBERFLÄCHE

Zusammenfassung—Der Einfluß zweier Anordnungen (fluchtend und versetzt) zylindrischer Rippen auf den Stoffübergang an einer ansonsten ebenen Oberfläche wird experimentell untersucht. Beide Anordnungen bestehen aus sieben Reihen kurzer Zylinder (Höhe = Durchmesser) mit gleichen Quer- und Längsteilungsverhältnissen. Die Naphthalin-Sublimations-Technik liefert in Verbindung mit einem automatisierten, rechnergesteuerten Meßsystem für die Naphthalin-Oberfläche detaillierte Informationen für den Stoffübergang. Die Verteilung der örtlichen Stoffübergangskoeffizienten deutet auf die Ausbildung periodisch wiederkehrender Bereiche sowie sich wiederholender örtlicher Maxima und Minima hin. Die Eigenheiten des Stoffübergangs unmittelbar am Fuß eines Zylinders in der Anordnung sind vergleichbar mit denjenigen in der Umgebung eines einzelnen isolierten Zylinders. Durch numerische Integration örtlicher Werte ergeben sich flächengemittelte Stoffübergangskoeffizienten, die einen direkten Vergleich zwischen zwei Anordnungen ermöglichen. Die Erhöhung des Stoffübergangs an der Oberfläche beträgt bei fluchtender Anordnung ungefähr 46%, bei versetzter Anordnung 53%.

ВЛИЯНИЕ РАСПОЛОЖЕНИЯ ЦИЛИНДРОВ, УСТАНОВЛЕННЫХ НА СТЕНКЕ, НА МАССОПЕРЕНОС ОТ ПЛОСКОЙ ПОВЕРХНОСТИ

Аннотация—Экспериментально исследуется влияние двух сборок цилиндров (с коридорным и шахматным расположением) на массоперенос от плоской пверхности, на которой они установлены. Обе сборки включают семь рядов цилиндров малой длины (отношение высоты к диаметру равно единице) с одинаковыми поперечными и продольными промежутками. С использованием методики, основанной на сублимации нафталина, в сочетании с автоматизированной системой измерений при помощи ЭВМ получена подробная информация о локальном массопереносе. Распределения локального коэффициента массопереноса позволяют определить механизм установления периодического режима с повторением локальных максимумов и минимумов. Характеристики массопереноса от области, непосредственно примыкающей к основанию цилиндра в сборке, согласуются с полученными для случая единичного изолированного цилиндра. Усредненные по площади результаты массопереноса, полученные методом численного интегрирования (суммирования) локальных данных, позволяют провести прямое, область за областью, сравнение процесса при обоих способах расположения цилиндров. При использовании сборок массоперенос от поверхности увеличивается примерно на 46% при коридорном расположении цилиндров и на 53%—при шахматном.